Image resolution enhancement via sparse interpolation on wavelet domain

Herminio Chávez-Román, Volodymyr Ponomaryov y Fernando Castro

H. Chavez, V. Ponomaryov y F. Castro
Universidad Tecnológica de la Región Norte de Guerrero, Iguala, Gro. bInstituto Politécnico Nacional, ESIME-Culhuacán, Ciudad de Mexico. México.
ochavezr@utrng.edu.mx

M. Ramos.,O. Rivas.,(eds.). Ciencias Multidisciplinarias, Proceedings-©ECORFAN- Valle de Santiago, Guanajuato, 2015

Abstract

The image processing algorithms collectively known as super-resolution (SR) have proven effective in producing high-quality imagery from low-resolution (LR) images. This paper focuses on a novel image resolution enhancement method employing the wavelet domain techniques. In order to preserve more edge information, additional edge extraction step is proposed employing high-frequency (HF) sub-band images - low-high (LH), high-low (HL), and high-high (HH) - via the Discrete Wavelet Transform (DWT). In the designed procedure, the LR image is used in the sparse interpolation for the resolution-enhancement obtaining low-low (LL) sub-band. Additionally, all sub-bands (LL, LH, HL and HH) are performed via the Lanczos interpolation. Finally, the estimated sub-band images are used to form the new high-resolution (HR) image using the inverse DWT (IDWT). Experimental results on real data sets have confirmed the effectiveness of the proposed framework in terms of objective criteria as well as in subjective perception.

21 Introduction

Relatively recently, researchers have begun developing methods to extend the SR algorithms to different imaging applications. There are differences that depend of imaging applications. Medical imaging applications differ from photographic imaging in several key respects. Unlike photographic imaging, medical imaging applications often use highly controlled illumination of the human subject during image acquisition that usually leads to higher signal-to-noise ratios (SNR). On other hand, the image processing artifacts are much less tolerable in medical images than in photographic applications. Another difference is that the majority of medical imaging applications involve creating images through three-dimensional objects. Thus, while the final images are two dimensional, they represent some form of projection through a three-dimensional volume [1].

The general image capture model, or forward model, combines the various effects of the digital image acquisition process such as point-wise blurring, motion, under-sampling, and measurement noise. The problem in this point is to estimate an HR image *u(m,n)* from measurements of an LR image *f(m,n)* that were obtained through a linear operator *K* that forms a degraded version of the unknown HR image, which was additionally contaminated by an additive noise $\mathcal{E}(m,n)$, and can be represented as the forward imaging model as follows:

$$f(m,n) = K[u(m,n)] + \mathcal{E}(m,n). \tag{21}$$

In most applications, *K* is a subsampling operator that should be inverted to restore an original image size and this problem usually should be treated as an ill-posed problem. Many image display devices have zooming abilities that interpolate input images to adapt their size to HR screens. Current proposal introduces a general class of nonlinear inverse estimators that were obtained with an adaptive mixing of linear estimators, with applications to image interpolation.

Wavelets also play a significant role in many image processing applications. The 2-D wavelet decomposition of an image is performed by applying the 1-D DWT along the rows of the image first, and then, the results are decomposed along the columns. This operation results in four decomposed sub-band images. The frequency components of those images in the sub-bands cover the full frequency spectrum of the original image. Image resolution enhancement using wavelets is a relatively new subject, and recently, many novel algorithms have been proposed [2-6]. These algorithms have attempted to improve the sharpness and fine features by using special procedures in the wavelet domain; where such reconstructions are performed by manipulations in the different decomposition sub-bands.

Prior information on the image sparsity has been widely used for image interpolation [7]. Wavelet estimators were introduced to compute fine-scale wavelet coefficients by extrapolating larger-scale wavelet coefficients [8, 9]. A more general and promising class of nonparametric SR estimators assumes that the HR image *u(m,n)* is sparse in some dictionary of vectors. This sparse representation is estimated by decomposing the LR measurements *f* in a transformed dictionary [10, 11]. The principal idea behind the restriction of the sparse SR algorithms is that the HR results can be improved by using more prior information on the image properties.

The predominant task of current study is consists of using an approach based on wavelet decomposition techniques that permit to take into account both spatial and spectral wavelet pixel information to enhance the resolution of a single image that can also be expanded to video sequences of different types [12, 13].

The principal contributions of current SR proposal in difference to other state of-the-art resolution-enhancement techniques consists in the mutual interpolation via *Lanczos* and Nearest-neighbor interpolation (*NNI)* techniques employed in *Wavelet Transform* (WT) HF sub-band images, an edge extraction procedure in wavelet transform space and adaptive directional LR image interpolation via sparse image mixture models in a DWT frame. The proposed framework additionally applies special denoising filtering that uses the *Non-Local Means* (NLM) for the input LR image performing better robustness in the SR process. Finally, all of the sub-band images are combined, generating a final HR image via IDWT that presents better resolution performance in terms of the objective criteria and subjective visual perception in comparison with the best existing algorithms.

To justify that the novel algorithm of image resolution enhancement has real advantages, we have compared the proposed SR procedure with other similar techniques, such as the following: *Demirel-Anbarjafari Super Resolution* (DASR) [14], *Wavelet domain image resolution enhancement using Cycle-Spinning* (WDIRECS) [15], *Image Resolution Enhancement applying Discrete and Stationary Wavelet Decomposition* (IREDSWD) [16], and *Discrete Wavelet Transform-Based Satellite Image Resolution Enhancement* (DWTSIRE) [17].

To ascertain the effectiveness of the proposed algorithm over other wavelet-domain resolution enhancement techniques, different LR images of different nature (satellite, medical and optical) obtained from [18, 19] were tested. The first database consists of the 20 medical images, and the second database contains 38 satellite images. All images have format of 8 bits/pixels for gray scale.

The remainder of this paper is organized as follows. Section 2.1 presents a short introduction to the NLM filtering method, Section 2.2 shows an implementation of an image interpolation through the inverse mixing estimator in a single image in wavelet space. The proposed technique for image SR reconstruction is presented in Section 3. Section 4 explains the applied quality criteria that were used to quantify the SR results. Section 5 discusses the qualitative and quantitative results of the proposed technique in comparison with other better conventional techniques. Finally, the conclusions are drawn in the final section.

19.1 Problem Statement Proposed Methodology

Non-Local Means Filtering

The NLM algorithm computes a denoised pixel $\hat{u}(m,n)$ by applying the weighted mean of the surrounding pixels of $f(m,n) = \{f(r,s)|(r,s) \in N(m,n)\}$, the estimated value for a pixel (m,n), is computed as a weighted average of all the pixels in the image [20]:

$$\hat{u}(m,n) = \frac{\sum_{(r,s)\in N(m,n)} f[r,s]w[m,n;r,s]}{\sum_{(r,s)\in N(m,n)} w[m,n;r,s]},$$

(21.1)

where $N(m,n)$ stands for the neighborhood of the pixel $f[r,s]$, and the term $w[m,n;r,s]$ is the weight for the *(m,n)-th* neighbor pixel.

The weights for the filter are computed based on radiometric (grey-level) proximity and geometric proximity between the pixels, namely:

$$w[m,n;r,s] = exp\left\{-\frac{(f[m,n]-f[r,s])^2}{2\gamma^2}\right\} \cdot g\left(\sqrt{(m-r)^2+(n-s)^2}\right).$$

(21.2)

The function g takes the geometric distance into account. The parameter γ controls the effect of the grey-level difference between the two pixels. This way, when the two pixels that is markedly different, the weight is very small, implying that this neighbor is not to be trusted in the averaging.

The denoised image $\hat{u}(m,n)$ is used in next steps of the proposed framework.

Interpolations with Sparse Wavelet Mixtures

The subsampled image $\hat{u}(m,n)$ is decomposed with one level DWT in the sub-bands (LL - approximations; and LH – horizontal details, HL – vertical details, HH diagonal details), which are treated as the matrixes H whose columns (approximations and details) are the vectors of a wavelet frame on a single scale. A construction is performed with a dual frame matrix H whose columns are the dual wavelet frames $\{h_{m,n}\}_{0\le m\le 3}$ [21]. The wavelet coefficients are written as follows:

$$\hat{z}(m,n) = \langle \hat{u}, h_{m,n}\rangle = H\hat{u}(m,n).$$

(21.3)

The WT separates an LF image (an approximation) z_l that is projected over the sub-band image *LL* scaling filters $\{h_{0,n}\}_{n\epsilon\mathcal{G}}$ and an HF image (details) z_h that is projected over the finest scale wavelets *LH*, *HL*, and *HH* in three directions $\{h_{m,n}\}_{1\le m\le 3, n\epsilon\mathcal{G}}$.

$$z_l = \sum_{n\epsilon\mathcal{G}} \hat{z}(0,n)h_{0,n} \quad and$$
$$z_h = \sum_{m=1}^{3} \hat{z}(m,n)h_{m,n}.$$

(21.4)

The LF image z_l has little aliasing, and it can be interpolated sufficiently well when applying a *Lanczos* interpolator V^+. For interpolating the HF image z_h, we employ directional interpolators V_θ^+ for $\theta\epsilon\Theta$, where Θ is a set of angles that is uniformly discretized between 0 and π.

For each angle θ, a directional interpolator V_θ^+ is applied over a block $D = D_{\theta,q}$ of wavelet coefficients if the directional regularity factor $\|\bar{Q}_D \hat{z}\|$; $\bar{Q}_D$ (sparse regularity operators) is relatively small in the mentioned block.

Such regularization is effective if the eigenvalues of the self-conjugated operator $\bar{Q}_D^* \bar{Q}_D$ have an overall variation that is sufficiently large to distinguish regular variations from non-regular variations in a given direction θ in *D*. For this step, it was proposed to choose rectangular blocks $D = D_{\theta,q}$ that are elongated in the direction of θ. Each block *D* in the spatial neighborhood of q is chosen to be identical in the three bands $d = 1,2,3$; thus, $l_D(m,n) = l_D(m)$, where l_D is the indicator of the approximation set *D*.

Each image $\hat{z}_D$ that is reconstructed from fine-scale wavelet coefficients in a block $D = D_{\theta,q}$ is interpolated with a directional interpolator $V_D^+ = V_\theta^+$. The HF residual $\hat{z}_r$ and the image LF f_l are interpolated with a separable and nearly isotropic *Lanczos* interpolator V^+. The resulting interpolator can be written in the following form [22]:

$$U_{LL} = V^+ \hat{z}(m,n) + \sum_{\theta \epsilon \Theta} (V_\theta^+ - V^+)\, \bar{\mathrm{H}} \left(\sum_{q \epsilon \bar{z}_\theta} \bar{a}\,(D_{\theta,q}) l_{D_{\theta,q}} \hat{z}(m,n) \right). \tag{21.5}$$

The image $\hat{z}(m,n)$ is first interpolated with a separable *Lanczos* interpolator V^+. For each angle θ, an update is computed over wavelet coefficients of each block of direction θ multiplied by their mixing weight $\bar{a}(D_{\theta,q})$, with the difference between the separable interpolator V^+ and a directional interpolator V_θ^+ along θ. This overall interpolator is calculated with $O(|\Theta|N)$ operations, where $|\Theta| = 20$ is the number of interpolation angles. Numerical experiments are performed with 20 angles, with blocks having a width of 2 pixels and a length between 6 and 12 pixels depending on their orientation.

Proposed approach in resolution enhancement

In this technique, one level of DWT that applies different wavelet families is used to decompose an input image. DWT separates an image into different sub-bands. The interpolation process should be applied to the four sub-band images.

Additionally, the novel framework applies a denoising procedure by using the *Non-Local Means* (NLM) for the input LR image (Noise Reduction Stage, Fig.21). This approach has better performance on the HF image components and generates significantly sharper and clearer edges and fine features in the final SR image.

In the proposed SR procedure, the LR image is used as the input data in the sparse representation for the resolution-enhancement process in the following way (Sparse Stage, Fig.21). Finally, the algorithm computes the missing samples along the direction θ from the previously calculated new samples, where the entire sparse process is performed with the *Lanczos interpolation*, reconstructing LL sub-band.

Figure 21 Block diagram of the proposed resolution-enhancement algorithm

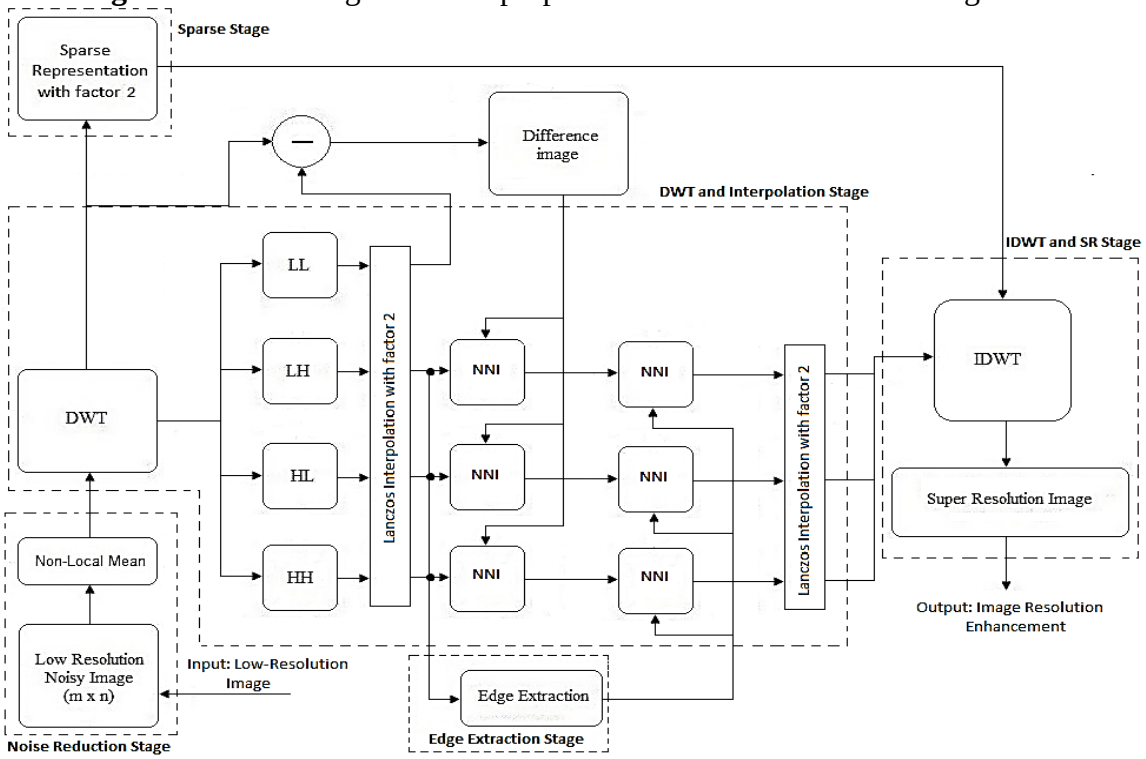

The differences between the interpolated LL sub-band image (with factor 2) and the LR input image are in their HF components that why it has been proposed the intermediate process to correct the estimated HF components applying this difference image. As it is seen in DWT and interpolation stage of the algorithm (Fig.21), this difference is performed in HF sub-bands by interpolating each band via NNI process (changing the values of pixels in agree with the closest neighbor value), including additional HF features into the HF images.

To preserve more edge information and to obtain a sharper enhanced image, we have proposed an extraction step of the edge using HF sub-bands images, that employs the first level in the DWT decomposition for an input image LR, the edge information is used into HF sub-bands employing NNI process (Edge Extraction Stage in Fig.21). The edge extracted image is calculated as follows [24]:

$$S = \sqrt{(HH)^2 + (HL)^2 + (LH)^2},$$

(21.6)

Finally, we perform an additional interpolation with *Lanczos* interpolation (factor 2) to reach the required size for the IDWT process (IDWT and SR Stage, Fig.21). It was noticed that the intermediate process of adding the difference image (the image that contains the HF components) generates a significantly sharper reconstructed SR image. This sharpness is boosted by the fact that the interpolation of the isolated HF components in HH, HL, and LH appears to preserve more HF components than interpolating from the LR image directly.

Performance evaluation

In order to evaluate the effectiveness of the proposed resolution enhancement algorithm, the following criteria are employed: *peak signal-to-noise ratio* (PSNR), *mean absolute error* (MAE), finally the *similarity structural index measure* (SSIM) [25, 26] which match better human subjectivity.

The PSNR is defined as:

$$PSNR = 10 \cdot log_{10} \frac{(255)^2}{MSE}, \text{dB},$$

(21.7)

Where, the mean square error (MSE) is the error measure for a gray scale image of dimension *mxn*.

The mean absolute error (MAE) is presented as follows:

$$MAE = \frac{1}{mxn} \sum_{i=1}^{m} \sum_{j=1}^{n} |\hat{u}[i,j] - u[i,j]|$$

(21.8)

To obtain the objective criteria value, PSNR and MAE employ the reference image (HR) $u(i,j)$ and the reconstructed SR image estimated via the SR algorithm $\hat{u}(i,j)$.

The standard quality metrics used in the past such as PSNR, can be erroneous in some cases; therefore, novel metrics, such as SSIM, which matches human subjectivity better, should be used to characterize the performance of the algorithm. For monochrome images, the SSIM metric values are defined as follows:

$$SSIM(u,\hat{u}) = \left[\frac{2\mu_{\hat{u}}\mu_u + C_1}{\mu_u^2 + \mu_{\hat{u}}^2 + C_1}\right] \cdot \left[\frac{2\sigma_{\hat{u}}\sigma_u + C_2}{\sigma_{\hat{u}}^2 + \sigma_u^2 + C_2}\right] \cdot \left[\frac{\sigma_{\hat{u}u} + C_3}{\sigma_{\hat{u}}\sigma_u + C_3}\right],$$

(21.9)

Here, $\hat{u}$ is the reconstructed SR image, and *x* is the original (HR) image; μ and σ^2 are the sample mean values and sample variances for the *u* or $\hat{u}$ images, and $\sigma_{\hat{u}u}$ is the sample cross-variance between the $\hat{u}$ and *u* images. The justification of the SSIM index can be found in [25, 26]. The constants C_1, C_2, and C_3 are used to stabilize the metric for the case in which the means and variances become very small, and usually $C_1=C_2=C_3=1$.

Because it is difficult to define the objective criteria that should be used to ensure the accurate quantization of the reconstructed images, a subjective measure of the image distortion was used in this study via subjective visual perception by human visual system. A subjective visual comparison of the images provides information about any spatial distortion or artifacts introduced by the algorithm that is employed and, thus, can make it possible to evaluate the performance of the analyzed technique in a different manner.

19.2 Experimental Results and Discussion

In order to show the effectiveness of the proposed method over the conventional and state-of-the-art image resolution enhancement techniques, different test images (*Baboon, Elaine, Aerial-A, Aerial-B, Medical-1* and *Medical-2*) with different feature are used for comparison from mentioned image databases. In this paper, the following families of classic wavelet functions are used: *Daubechies* (Db), *Symlet* (Sym), and *biorthogonal* (Bior).

Referring to the image *Baboon (*Fig.21.1) shows the results of the SR reconstruction algorithm applied to a LR 128×128 pixels image to obtain a 512x512 pixels resolution enhancement image. The novel resolution enhancement algorithm appears to perform better in terms of objective criteria (PSNR and SSIM) as well as in terms of subjective perception, especially using wavelet *Db-1*. The visual subjective perception can be verified in the zoomed part of the *Baboon* image (left eye), where fine details appear to be preserved better in the novel proposed SR framework.

In the SR reconstructed *Elaine* image, one can observe from analyzing Fig. 21.2 that the novel algorithm performs better in PSNR and SSIM, especially using wavelet *Sym-2*, also it presents the better perception especially in the well-defined borders (see the zoomed part of the image).

Figure 21.1 Visual perception results for the Baboon image contaminated by Gaussian noise (PSNR=17 dB)

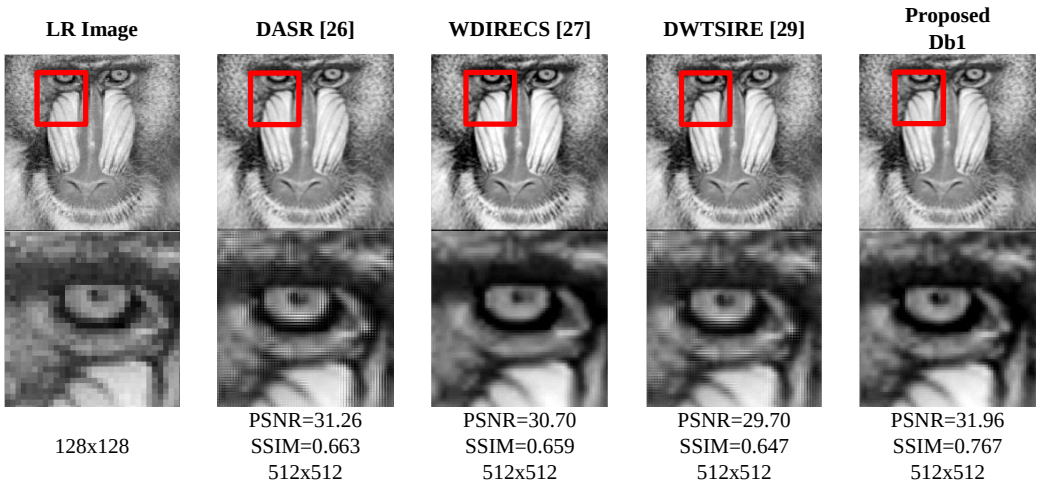

Figure 21.2 Visual perception results for the Elaine image contaminated by Gaussian noise (PSNR=17 dB)

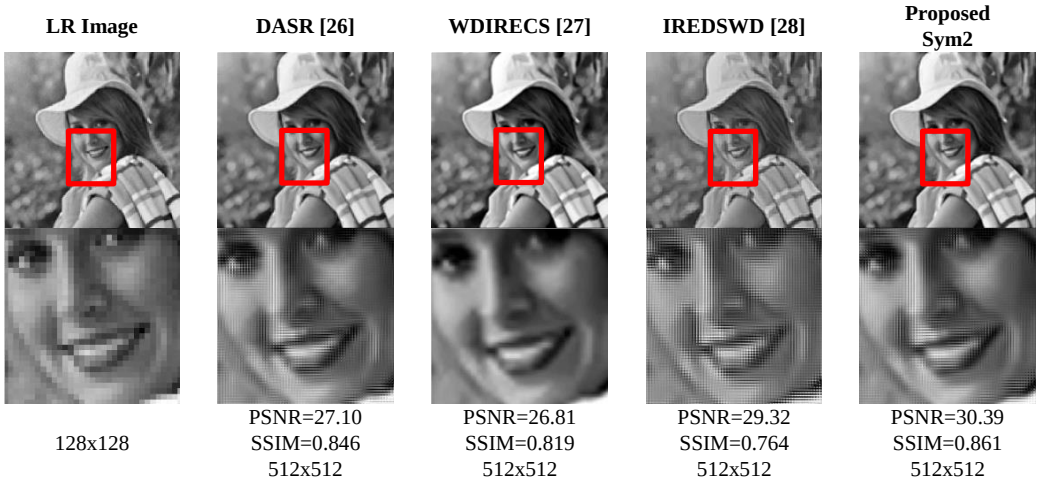

Figure 21.3 Visual perception results for the Aerial-A image contaminated by Gaussian noise (PSNR=17 dB)

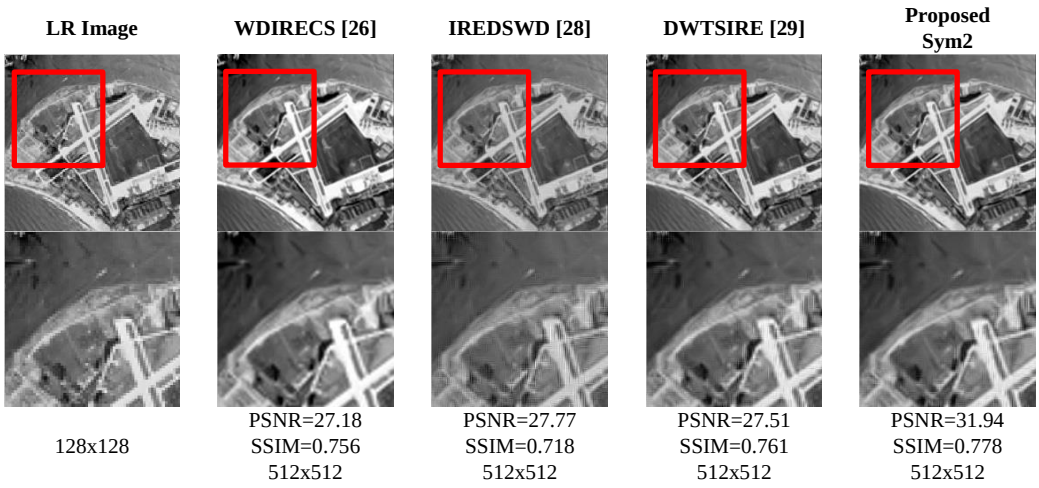

Figure 21.4 Visual perception results for the Aerial-B image contaminated by Gaussian noise (PSNR=17 dB)

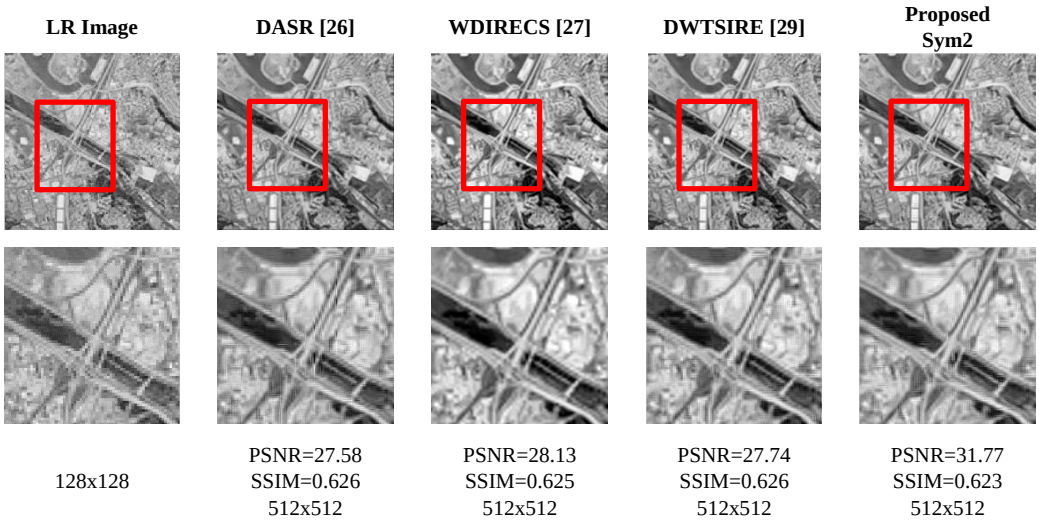

In the resolution enhancement of the *Aerial-A* image (see Fig.21.3), one can observe that there is better performance in terms of the objective criteria PSNR and SSIM as well as in the subjective perception when the proposed SR procedure is employed with the wavelet *Sym-2* in comparison with the other state-of-the art technique.

Fig. 5 compares the *Aerial-B* image obtained by different algorithms. In the zoomed images, one can observe that conventional SR methods produce some blur and artifacts. In contrast, the novel SR algorithm provides better image quality (PSNR and SSIM), when the wavelet *Sym-2* is employed. The proposed SR algorithm restores slightly better regular geometrical structures.

The resolution enhancement algorithms have an important application in the processing of medical images. For this reason, we have tested several medical images. In the *Medical-1* image (see Fig. 6), it is easy to see better performance in accordance with the objective criteria and via subjective visual perception in SR enhancement when the proposed algorithm is employed with the wavelet *Sym-2*. Better preservation of the fine details in the zoomed part of the image can be obtained for the novel resolution enhancement framework.

Fig. 21.6 compares the SR image *Medical-2* obtained by different algorithms. In the zoomed images, one can observe that conventional SR methods produce some blur and artifacts. In contrast, the novel proposed algorithm provides better image quality (PSNR and SSIM), when the wavelet *Sym-2* is employed. The proposed algorithm restores slightly better regular geometrical structures, as shown in the zoomed part in *Medical-2*.

Figure 21.5 Visual perception results for the Medical-1 image contaminated by Gaussian noise (PSNR=17 dB)

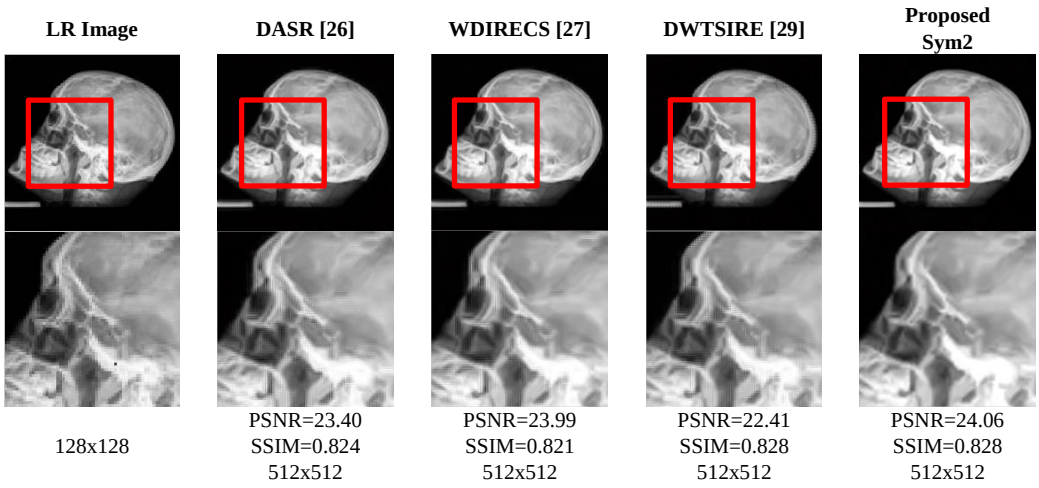

Figure 21.6 Visual perception results for the Medical-2 image contaminated by Gaussian noise (PSNR= 17 dB)

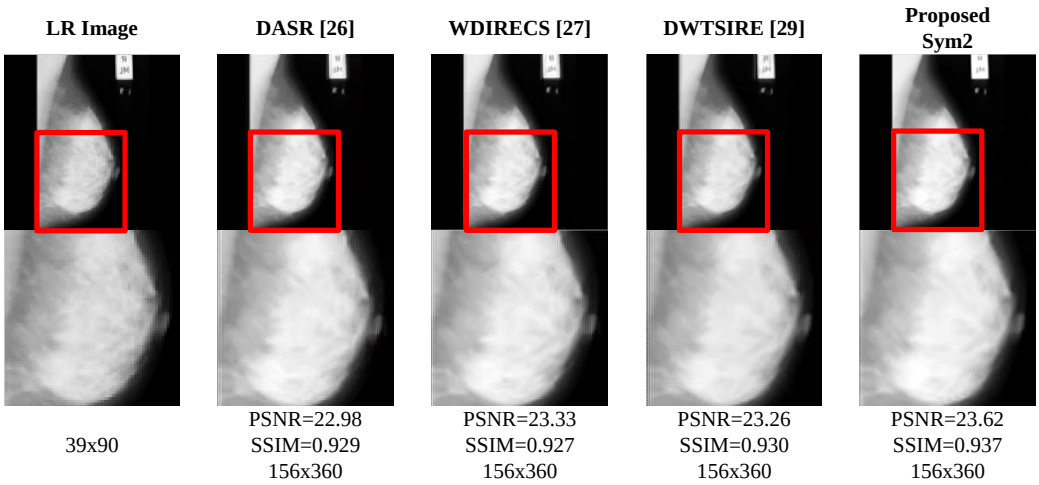

In these experiments, we revise the resolution enhancement of a number of images from databases. It can be concluded from this analysis of the SR enhancement images that novel framework results in sharper edges and fine features, better cleaning in details, and visually closely resembles the original image when it compares against the other techniques SR results. Overall, the results in table 21, 21.1, 21.2 and 21.3 show the better performance in terms of the objective criteria (PSNR, MAE and SSIM) as well as in the subjective perception via human visual system.

Table 21 Objective criteria values of the resolution enhancement from 128x128 to 512x512. (The LR image is contaminated by Gaussian noise PSNR=17 dB)

Sr Methods		**Baboon**			**Elaine**		
		Mae	**Psnr**	**Ssim**	**Mae**	**Psnr**	**Ssim**
Iredswd [16]	**Db1**	7.968	31.055	0.648	7.547	29.433	0.764
	Sym2	7.677	30.909	0.589	7.117	29.320	0.764
	Bior1.3	9.178	30.295	0.626	8.340	28.181	0.744
Dwtsire [17]	**Db1**	8.192	29.702	0.647	8.020	26.830	0.824
	Sym2	10.864	29.450	0.640	7.481	27.625	0.861
	Bior1.3	10.967	29.288	0.532	7.207	26.982	0.786
Dasr [14]	**Db1**	6.833	31.261	0.663	7.273	26.748	0.805
	Sym2	7.325	30.985	0.647	7.986	27.106	0.846
	Bior1.3	7.191	31.158	0.654	7.557	26.745	0.804
Wdirecs [15]	**Db1**	7.263	30.700	0.659	7.490	26.681	0.767
	Sym2	6.260	31.357	0.657	6.199	26.814	0.819
	Bior1.3	7.244	30.709	0.659	7.554	26.667	0.766
Proposed Sr Technique	**Db1**	**5.412**	**31.968**	**0.767**	6.951	30.256	0.835
	Sym2	5.557	32.137	0.620	**5.561**	**30.398**	**0.861**
	Bior1.3	5.585	31.898	0.716	6.429	30.484	0.829

Table 21.1 Objective criteria values of the resolution enhancement from 128x128 to 512x512. (The LR image is contaminated by Gaussian noise PSNR=17 dB)

Sr Methods		**Aerial-A**			**Aerial-B**		
		MAE	**PSNR**	**SSIM**	**MAE**	**PSNR**	**SSIM**
Iredswd [16]	**Db1**	13.163	26.215	0.659	21.561	26.971	0.515
	Sym2	12.834	27.770	0.718	19.198	27.022	0.577
	Bior1.3	14.012	27.117	0.692	19.115	27.106	0.433
Dwtsire [17]	**Db1**	13.524	27.521	0.688	19.521	27.312	0.543
	Sym2	11.530	27.510	0.761	16.988	27.739	0.626
	Bior1.3	13.442	27.130	0.682	20.617	27.265	0.539
Dasr [14]	**Db1**	16.371	27.305	0.685	19.841	27.442	0.540
	Sym2	15.858	27.176	0.758	18.167	27.578	0.626
	Bior1.3	17.113	27.125	0.676	20.707	27.313	0.532
Wdirecs [15]	**Db1**	13.992	27.311	0.673	16.957	27.726	0.532
	Sym2	12.028	27.718	0.756	14.493	28.130	0.625
	Bior1.3	13.946	27.318	0.674	16.920	27.736	0.532
Proposed Sr Technique	**Db1**	7.631	30.953	0.734	7.315	31.111	0.583
	Sym2	**5.542**	**31.946**	**0.778**	**5.858**	**31.774**	**0.623**
	Bior1.3	6.813	31.261	0.729	6.477	31.363	0.580

Table 21.2 Objective criteria values of the resolution enhancement from 128x128 to 512x512. (The LR image is contaminated by Gaussian noise PSNR=17 dB)

Sr Methods		**Medical-1**			**Medical-2**		
		MAE	**PSNR**	**SSIM**	**MAE**	**PSNR**	**SSIM**
Iredswd [16]	**Db1**	14.929	18.918	0.786	9.821	20.415	0.906
	Sym2	10.921	22.350	0.819	8.536	22.621	0.915
	Bior1.3	14.269	19.600	0.747	11.806	19.959	0.889
Dwtsire [17]	**Db1**	11.138	21.841	0.804	10.192	22.181	0.915
	Sym2	9.959	22.412	0.828	8.379	23.259	0.930
	Bior1.3	11.753	20.212	0.797	9.500	22.178	0.916
Dasr [14]	**Db1**	11.154	21.786	0.807	10.180	22.175	0.916
	Sym2	10.217	23.399	0.824	8.793	22.977	0.929
	Bior1.3	11.395	21-628	0.792	10.213	22.090	0.915
Wdirecs [15]	**Db1**	10.904	22.297	0.811	9.671	22.395	0.929
	Sym2	10.131	23.987	0.821	8.616	23.334	0.927
	Bior1.3	10.924	22.863	0.805	9.743	22.534	0.929
Proposed Sr Technique	**Db1**	10.699	22.442	0.812	9.599	22.924	0.934
	Sym2	**9.844**	**24.063**	**0.828**	**8.365**	**23.625**	**0.937**
	Bior1.3	10.830	22.288	0.809	9.612	22.909	0.934

Numerous statistical simulations that we realized using databases that contain the test images of different nature (satellite, medical, optical, etc.) that are characterized by varying texture, details and edges, properties have confirmed the better performance of proposed method in resolution enhancement guaranteeing it robustness.

21.3 Conclusions

In this work, a novel resolution-enhancement technique based on the interpolation of the HF sub-band images in the wavelet domain is presented. In contrast with other state-of-the-art resolution-enhancement techniques, the designed framework applies the edge and fine features information that is obtained from the HF sub-band images in wavelet transform space, NLM denoising algorithm modifying them for the SR restoration, and performs the sparse interpolation over an oriented block (approximations and details) in an LR image. All of these steps result in image resolution enhancement.

Numerous simulation results on images from databases of different nature (satellite, medical, optical) have confirmed superiority of the proposed enhancement framework in performing the SR reconstruction while employing different wavelet function in comparison with other conventional methods. Experimental results have demonstrated better performance and robustness of the proposed algorithm in terms of objective criteria (PSNR, MAE and SSIM), as well as in the subjective perception via the human visual system.

21.4 References

Castillejos, H., Ponomaryov, V., Nino-de-Rivera, L. and Golikov, V., "Wavelet Transform Fuzzy Algorithms for Dermoscopic Image Segmentation," Computational and Mathematical Methods in Medicine, doi: 10.1155/2012/578721, (2012).

X. Li and M. T. Orchard (2001), "New edge-directed interpolation". *IEEE Trans. Image Process*. vol. 10, No. 10, pp. 1521–1527.

K. Kinebuchi, D. D. Muresan, and T. W. Parks (2001), "Image interpolation using wavelet based hidden Markov trees", in *Proc. IEEE ICASSP*, vol. 3, pp. 7–11.

S. Zhao, H. Han, and S. Peng (2003), "Wavelet domain HMT-based image super resolution", *Proc. IEEE ICIP*, Vol. 2, pp. 933–936.

A. Temizel and T. Vlachos (2005), "Image resolution up-scaling in the wavelet domain using directional cycle spinning," *J. Electron. Imaging,* Vol. 14, No. 4, p. 040501.

A. Gambardella and M. Migliaccio (2008), "On the super-resolution of microwave scanning radiometer measurements", *IEEE. Trans. Geoscience and Remote Sensing* Letters, Vol. 5, No. 4, pp. 796–800.

M. Elad, M. A. T. Figueiredo, and Y. Ma. (2010) "On the role of sparse and redundant representations in image processing". Proc. of IEEE, 98(6):972–982.

Chavez-Roman, H. and Ponomaryov. V., "Super Resolution Image Generation Using Wavelet Domain Interpolation with Edge Extraction Via a Sparse Representation," IEEE Geoscience and Remote Sensing Letters, doi: 10.1109/LGRS.2014.2308905, (2014).

H. Chavez, V. Gonzalez, A. Hernandez, and V. Ponomaryov "Super Resolution Imaging via Sparse Interpolation in Wavelet Domain with Implementation in DSP and GPU", Lecture Notes in Computer Science, LNCS 8827, pp. 973–981, 2014.

M. Elad, J. L. Starck, P. Querre, and D. L. Donoho (2005), "Simultaneous cartoon and texture image inpainting using morphological component analysis (MCA)," Appl. Comput. Harmon. Anal, vol. 19, pp. 340–358.

M. J. Fadili, J. L. Starck, and F. Murtagh (2007), "Inpainting and zooming using sparse representations," Comput. J.

V. Kravchenko, H. Meana, and V. Ponomaryov (2009), "*Adaptive Digital Processing of Multidimensional Signals with Applications"*, FizMatLit, Edit, Moscow, Russia, http://www.posgrados.esimecu.ipn.mx/.

E. Ramos, V. F. Kravchenko and V. Ponomaryov (2011), "Efficient 2D to 3D video conversion implemented on DSP", *EURASIP Journal on Advances in Signal Processing,* doi:10.1186/1687.

G. Anbarjafari and H. Demirel (2010), "Image Super Resolution Based on Interpolation of Wavelet Domain High Frequency Sub-bands and the Spatial Domain Input Image", *ETRI Journal,* vol. 32, No. 3, pp. 390-394.

Temizel A. and Vlachos T. (2005), "Wavelet domain image resolution enhancement using cycle-spinning", Elect. Lett.,vol. 41, Issue 3, pp.:119 – 121.

H. Demirel and G. Anbarjafari (2011), "Image Resolution Enhancement by Using Discrete and Stationary Wavelet Decomposition", *IEEE Trans. Image Processing,* Vol. 20, Is. 5, pp. 1458-1460.

H. Demirel and G. Anbarjafari (2011), “Discrete Wavelet Transform-Based Satellite Image Resolution Enhancement”, *IEEE Trans. Geoscience and Remote Sensing*, Vol. 49, Is. 6, pp. 1997-2004.
http://peipa.essex.ac.uk/benchmark/databases/index.html
http://sipi.usc.edu/database/

M. Protter, M. Elad, H. Takeda, and P. Milanfar (2009), “Generalizing the nonlocal-means to super-resolution reconstruction,” *IEEE Trans. Image Process.*, vol. 18, no. 1, pp. 36–51.

A. Buades, B. Coll, and J. M. Morel (2005), “A review of image denoising algorithms, with a new one,” Multisc. Model. Simul., vol. 4, no. 2, pp. 490-530.

S. Mallat and G. Yu (2010), “Super-Resolution with Sparse Mixing Estimators”, IEEE Trans. on Image Process. Vol.19, Issue 11 pp.2889-2900. DOI: 10.1109/TIP.2010.2049927.

S. Mallat (2008), “A Wavelet Tour of Signal Processing: The Sparse Way”, 3rd ed. New York: Academic.

L. Feng, C. Y. Suen, Y.Y. Tang and L.H. Yang (2000), “Edge Extraction of Images by Reconstruction Using Wavelet Decomposition Details at Different Resolution Levels”, Int J. Patt. Recogn. Artif. Intell.,Vol.14, Issue 6, pp. 779-793. DOI: 10.1142/S0218001400000519.

Z. Wang, A. Bovik (2009), “Mean Squared Error: Love It or Leave It? A new look at signal fidelity measures,” IEEE Signal Proc. Magazine, Vol.26, No.1, pp. 98-117.

Z.Wang, A. Bovik, H. Seikh and E. Simoncelli (2004), “Image Quality Assessment: From Error Visibility to Structural Similarity”. IEEE Trans. Image Process., vol. 13, No. 4, pp. 600-612.